

Improving the speed of variational quantum algorithms for quantum error correction

Fabio Zoratti

Scuola Normale Superiore, I-56126 Pisa, Italy

Giacomo De Palma

Department of Mathematics, University of Bologna, 40126 Bologna, Italy

Vittorio Giovannetti

NEST, Scuola Normale Superiore and Istituto Nanoscienze-CNR, I-56126 Pisa, Italy

We consider the problem of devising a suitable quantum error correction procedure for a generic quantum noise acting on a quantum circuit. In general, there is no analytic universal procedure to obtain the encoding and correction unitary gates, and the problem is even harder if the noise is unknown and has to be reconstructed. The existing procedures rely on variational quantum algorithms and are very difficult to train since the size of the gradient of the cost function decays exponentially with the number of qubits. We address this problem using a cost function based on the quantum Wasserstein distance of order 1. Our results show that such cost function significantly increases both the probability of a successful training and the fidelity of the recovered state.

I. INTRODUCTION

Performing reliable computations on physical imperfect hardware is something that has become usual nowadays, given the current state of classical computers, which can produce perfect results without any software-side mitigation of the imperfections of the physical media where the computation happens. Error correction is based on the fact that these machines perform automatically, on the hardware side, procedures that allow errors to happen and to be fixed without any intervention of the end user. This kind of setting is even more crucial in a quantum scenario where the current noisy intermediate-scale quantum computers (NISQ) have a much larger error rate than their classical counterparts [1]. Performing reliable computations with a trustworthy error correction procedure has direct implications not only in quantum computation [2, 3], but also in quantum key distribution and cryptography [4–8].

In the typical Quantum Error Correction (QEC) scheme, the quantum state that has to be protected is stored in a subspace of a larger Hilbert space, using an *encoding* procedure. Stabilizer codes [9], which are within the best analytical results in this field, are not universal because they are tailored for a generic noise acting on a small but unknown subset of qubits. Several attempts have already been made to create a numerical optimization procedure to find an error correction code for specific noise models [10–13], but these studies are not universal because they rely heavily on the type of noise on the specific quantum circuit and this is a problem because real quantum devices are not characterized by a single kind of quantum noise. Some attempts have been made to characterize the noise of the current and near-term devices [14, 15], but these methods will become very difficult to implement soon because classical computers are not able to simulate efficiently quantum circuits when

the number of qubit increases. Near-term devices with approximately 50 qubits may already be intractable to simulate for supercomputers [16].

If we define a figure of merit of the quality of the state after the action of the noise and its corresponding correction, the obvious choice for the kind of maximization algorithm is a Variational Quantum Algorithm [17]. These are hybrid algorithms that couple a quantum computer with a classical one. In this kind of algorithms, usually, a parametric quantum circuit is applied to some reference state, some measurements are performed on the system, and the outcomes are given to the classical computer to perform a minimization procedure of a given cost function. Some interesting examples of this class of algorithms are the variational quantum eigensolver [18] and the Quantum Approximate Optimization Algorithm (QAOA) [19]. The optimization procedure in a variational quantum algorithm can be seen as the training phase in machine learning, for example, to train a neural network.

Some variational quantum algorithms applied to quantum error correction are already known in literature [20]. However, VQAs usually suffer from the phenomenon of barren plateaus [21, 22], namely the gradient of the cost function decays exponentially with respect to the number of qubits of the system, leading to an untrainable model. Some general results have already been found about this topic [22], which justifies the presence of barren plateaus when the cost function is a global function of the quantum circuit, namely the measurement of a highly non-local operator. For this reason, we compared the performance of an algorithm inspired by [20] using two different cost functions: the fidelity and an approximation of the quantum Wasserstein distance.

The quantum Wasserstein distance is a generalization of the classical Wasserstein distance between probability distributions [23–27]. Several quantum generalizations of the Wasserstein distance have been proposed [28–62]. This

work is based on the quantum Wasserstein distance of order 1 (or quantum W_1 distance) proposed in Refs. [63, 64], which is not unitarily invariant and recovers the Hamming distance [65] for the states of the computational basis. We expect this new distance to improve the barren plateau phenomenon and we can give an intuitive reason. If we use a unitarily invariant distance as the trace distance or the distances derived from the fidelity, all the states of the computational basis are equally orthogonal and thus have all maximum distance one with respect to the other. The quantum W_1 distance instead measures how many qubits are different between the two states and this allows the gradient to be less flat in the regions that are not already very close to a local minimum. Indeed, the quantum W_1 distance has successfully been employed as cost function of quantum Generative Adversarial Networks [64, 66–70]

The manuscript is organized as follows: in Sec. II we present some basic notion on conventional QEC procedures which allow us to set the notation and the theoretical background; in Sec. III we introduce our VQA discussing the different choices of cost functions that can be used in order to guide it; in Sec. IV we present our numerical results where comparing the performances of the VQA implemented with different types of cost functions. Conclusions are given in Sec. V.

II. PRELIMINARIES ON QEC

Let Q be a quantum register we wish to protect (at least in part) from the action of some external noise source. In a typical QEC scenario [71] this problem is addressed through the following three-step procedure:

- i)* Before the action the noise, a unitary encoding gate \hat{V}_{QA} is used to distribute the information originally contained in Q on the larger system QA . Here A is an auxiliary quantum register that is assumed to be initialized in a fiduciary quantum state, and that is affected by the same noise that tampers with Q ;
- ii)* After the action of the noise a measurement on QA is performed to reveal the nature of the latter and, based on the associated outcome, a unitary recovery operation is applied to the system. Equivalently this step can be described by introducing yet an extra quantum register B (also initialized on a fiduciary state but *not* affected by the noise) that is coupled with QA through a recovering unitary transformation \hat{W}_{QAB} which effectively mimics the measurement and the recovery operation;

- iii)* The inverse of the gate \hat{V}_{QA} is finally used on QA to refocus the recovered information in Q .

Denoting with $|\psi\rangle_Q$ the input state of Q , the corresponding output state of QA that emerges from the process at the end of the step *iii)* can be expressed as the

density matrix

$$\begin{aligned} \hat{\rho}_{QA}^{(V,W)}(\psi) &:= \text{tr}_B \left\{ \mathcal{V}_{QA}^\dagger \circ \mathcal{W}_{QAB} \circ \Phi_{QA} \right. \\ &\quad \left. \circ \mathcal{V}_{QA} \left(|\psi\rangle_Q \langle \psi| \otimes |\mathcal{O}\rangle_A \langle \mathcal{O}| \otimes |\mathcal{O}\rangle_B \langle \mathcal{O}| \right) \right\} \\ &:= \mathcal{V}_{QA}^\dagger \circ \Phi_{QA}^{(R)} \circ \Phi_{QA} \circ \mathcal{V}_{QA} \left(|\psi\rangle_Q \langle \psi| \otimes |\mathcal{O}\rangle_A \langle \mathcal{O}| \right) \end{aligned} \quad (1)$$

where $|\mathcal{O}\rangle_X$ represents the fiduciary state of the X register, $\text{tr}_B\{\dots\}$ is the partial trace over B , and given a unitary \hat{U}_X on X we adopted the symbol $\mathcal{U}_X(\dots) := \hat{U}_X \dots \hat{U}_X^\dagger$ to denote its action as super-operator. In the above expressions Φ_{QA} is the LCPT quantum channel [71] describing the noise on Q and A , while $\Phi_{QA}^{(R)}(\dots) := \text{tr}_B\{\mathcal{W}_{QAB}(\dots \otimes |\mathcal{O}\rangle_B \langle \mathcal{O}|)\}$ is the LCPT (recovery) quantum channel on QA originating from the interaction with B , that attempts to undo the action of Φ_{QA} .

An ideal QEC procedure capable to completely remove the noise from the system will make sure that $\hat{\rho}_{QA}^{(V,W)}(\psi)$ corresponds to $|\psi\rangle_Q |\mathcal{O}\rangle_A$, irrespectively from the specific choice of $|\psi\rangle_Q$. A bona-fide figure of merit to characterize the effectiveness of a generic QEC scheme is hence provided by the average input-output fidelity

$$\bar{F}(V, W) := \int d\mu_\psi \, {}_Q\langle \psi | {}_A\langle \mathcal{O} | \hat{\rho}_{QA}^{(V,W)}(\psi) | \psi \rangle_Q | \mathcal{O} \rangle_A, \quad (2)$$

where $d\mu_\psi$ is the uniform measure on the set of the input states of Q originated from the Haar measure on the associated unitary group [72] or from an exact or approximate unitary 2-design \mathcal{S} [71, 73] that simulates the latter¹. Notice that by expressing $|\psi\rangle_Q = \hat{U}_Q |\mathcal{O}\rangle_Q$, Eq. (2) can equivalently be casted in the more compact form

$$\bar{F}(V, W) = {}_QA\langle \mathcal{O} | \hat{\rho}_{QA}^{(V,W)} | \mathcal{O} \rangle_{QA}, \quad (3)$$

with $|\mathcal{O}\rangle_{QA} := |\mathcal{O}\rangle_Q \otimes |\mathcal{O}\rangle_A$ and where the state

$$\begin{aligned} \hat{\rho}_{QA}^{(V,W)} &:= \frac{1}{|\mathcal{S}|} \sum_{\hat{U}_Q \in \mathcal{S}} \mathcal{U}_Q^\dagger \circ \mathcal{V}_{QA}^\dagger \circ \Phi_{QA}^{(R)} \circ \Phi_{QA} \\ &\quad \circ \mathcal{V}_{QA} \circ \mathcal{U}_Q \left(|\mathcal{O}\rangle_{QA} \langle \mathcal{O}| \right), \end{aligned} \quad (4)$$

now includes the average over all possible inputs. An ideal QEC procedure will enable one to get $\bar{F}(V, W) = 1$. A natural benchmark for lowest admissible $\bar{F}(V, W)$ is represented instead by the value one would get if one decides not to perform corrections on the register that we

¹ We remind that a unitary 2-design is a probability distribution over the set of unitary operators which can duplicate properties of the probability distribution over the Haar measure for polynomials of degree 2 or less. When Q is a single qubit, a 2-design can be realized by a uniform sampling over a set \mathcal{S} composed by only 6 elements $\hat{\mathbb{1}}, \hat{\sigma}_1, e^{\pm i\pi/4\hat{\sigma}_1}, e^{\pm i\pi/4\hat{\sigma}_2}$ that maps its logical state $|\mathcal{O}\rangle_Q$ into the vectors $|\mathcal{O}\rangle_Q, |1\rangle_Q, (|\mathcal{O}\rangle_Q \pm i|1\rangle_Q)/\sqrt{2}, (|\mathcal{O}\rangle_Q \mp |1\rangle_Q)/\sqrt{2}$.

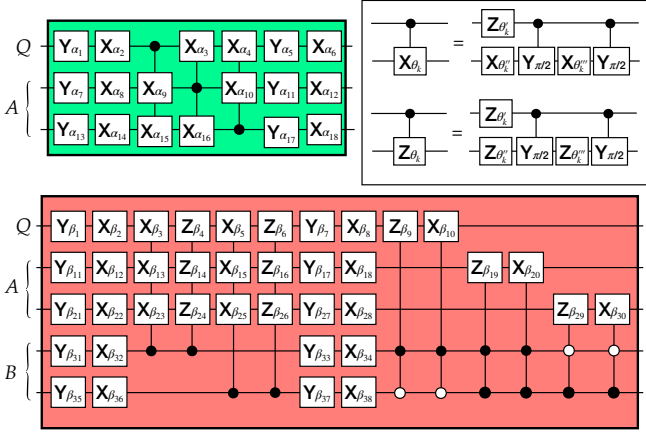


Figure 1. Parametric gates $\hat{V}_{QA}(\vec{\alpha})$ (green element) and $\hat{W}_{QAB}(\vec{\beta})$ (red element) used for case of quantum registers Q , A , and B with $k = 1$, $n - k = 2$, and $r = 2$ qubits respectively. Indicating with $\hat{\sigma}_1, \hat{\sigma}_2$, and $\hat{\sigma}_3$ the Pauli operators, the X_θ, Y_θ , and Z_θ elements of the figure represent single qubit rotations $e^{-i\theta\hat{\sigma}_1}, e^{-i\theta\hat{\sigma}_2}$, and $e^{-i\theta\hat{\sigma}_3}$ with the angles θ determined to the components of the vectors $\vec{\alpha}, \vec{\beta}$, respectively. Vertical lines indicate instead quantum control operations which are activated when the control qubits (indicated by the full or empty circles) are in the logical state $|1\rangle$ (full circle) or in $|0\rangle$ (empty circle). As shown on the inset, each one of those gates depend parametrically upon elements of the control vectors $\vec{\alpha}$ and $\vec{\beta}$ through single qubit operations.

compute by setting \hat{V}_{QA} and \hat{W}_{QAB} equal to the identity operators i.e.²

$$\bar{F}_0 := {}_Q\langle\mathcal{O}|\hat{\rho}_{QA}^{(\mathbb{I},\mathbb{I})}|\mathcal{O}\rangle_{QA}. \quad (5)$$

III. VARIATIONAL QUANTUM ALGORITHM

While the enormous progress has been made in the study of QEC procedures, identifying efficient choices for the operations that leads to (non trivial) high values of $\bar{F}(V, W)$ for a specific noise model, is still a challenging open problem. A possible solution in this case is to employ variational quantum algorithms to run numerical searches. Our approach follows a training strategy inspired by the work of Johnson *et al.* [20]. Assuming hence Q , A , and B to be formed by collections of independent qubits (k for Q , $n - k$ for A , and r for B), we introduce a manifold

² Equation (5) accounts for the noise effects both on Q and A . A more conservative estimation of \bar{F}_0 can be obtained by focusing directly on the noise on Q alone, i.e. tracing out the A component of $\hat{\rho}_{QA}^{(\mathbb{I},\mathbb{I})}$ and studying its fidelity with $|\mathcal{O}\rangle_Q$, i.e. $\bar{F}_0^{(\text{strong})} := {}_Q\langle\mathcal{O}|\hat{\rho}_Q^{(\mathbb{I},\mathbb{I})}|\mathcal{O}\rangle_Q \geq \bar{F}_0$, with $\hat{\rho}_Q^{(\mathbb{I},\mathbb{I})} := \text{tr}_A \hat{\rho}_{QA}^{(\mathbb{I},\mathbb{I})}$. Notice that for the noise model of Sec. III C the two are directly connected via the identity $\bar{F}_0 = \bar{F}_0^{(\text{strong})} - \frac{n-1}{n}p(1 - |\langle\mathcal{O}|\hat{\sigma}|\mathcal{O}\rangle|^2)$.

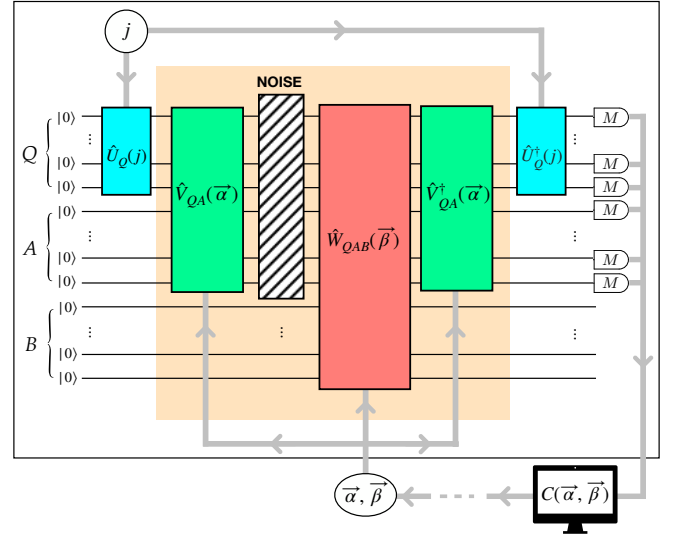


Figure 2. (Color online) Sketch of the variational quantum algorithm: Q , A and B are quantum registers formed respectively by k , $n - k$ and r qubits. The initial information we wish to protect is written in Q by the unitary gate $\hat{U}_Q(j)$ extracted from a 2-design set \mathcal{S} ; A and B are two auxiliary elements (containing respectively $n - k$ and r qubits) that are used to implement the QEC procedure described by the parametric gates $\hat{V}_{QA}(\vec{\alpha})$, $\hat{W}_{QAB}(\vec{\beta})$, and $\hat{V}_{QA}^\dagger(\vec{\alpha})$ of Fig. 1. The patterned element in the central part of the scheme represents the noise on Q and A (no noise is assumed to be active on B). Lastly, the D-shaped measurements at the end of the circuit represent local measurements on QA whose outcomes over the entire collection of the possible inputs generated by the entire set \mathcal{S} , are processed by a classical computer which, evaluating the cost function $C(\vec{\alpha}, \vec{\beta})$ defined in Section III B, decides how to update the values of the parameters $\vec{\alpha}$ and $\vec{\beta}$. Thick grey lines in the figure represent classical control lines.

of transformations $\hat{V}_{QA}(\vec{\alpha})$, $\hat{W}_{QAB}(\vec{\beta})$ parametrized by classical controls vectors $\vec{\alpha}, \vec{\beta}$ (see Fig. 1), and construct the quantum circuit of Fig. 2. The method then proceeds along the following stages:

1. Having selected the values of $\vec{\alpha}$ and $\vec{\beta}$, the register Q is prepared into a collection of known quantum state $\{|\psi(1)\rangle_Q, \dots, |\psi(m)\rangle_Q\}$ operating on the vector $|\mathcal{O}\rangle_Q = |0\rangle^{\otimes k}$ through action of the control gates $\hat{U}_Q(1), \dots, \hat{U}_Q(m)$ (first cyan element of the figure) which define the 2-design \mathcal{S} entering in Eq. (4). Each of such inputs is hence evolved via a circuit (pale-orange area of the figure) that emulates both the effect of the noise (patterned square of the figure, see Section III C and Fig. 4), and the transformations $\hat{V}_{QA}(\vec{\alpha})$, $\hat{W}_{QAB}(\vec{\beta})$, and $\hat{V}_{QA}^\dagger(\vec{\alpha})$ that are meant to implement the steps *ii*) and *iii*) of the QEC procedure (green and red elements of the figure). Notice that in the ideal case (i.e. if $\hat{V}_{QA}(\vec{\alpha})$ and $\hat{W}_{QAB}(\vec{\beta})$ manage to completely suppress the noise) then in correspondence with

the input $|\psi(j)\rangle_Q$ the registers QA should emerge in the state $|\psi(j)\rangle_Q \otimes |\mathcal{O}\rangle_A := |\psi(j)\rangle_Q \otimes |0\rangle^{\otimes n-k}$, which will be hence mapped into the final configuration $|\mathcal{O}\rangle_{QA} := |0\rangle^{\otimes n}$ by the inverse $\hat{U}_Q^\dagger(j)$ of the state preparation gate (second cyan element of the figure).

2. For each choice of the index $j \in \{1, \dots, m\}$ a measurement on the system is performed at the end of the transformations described in the stage 1 and the resulting m collected outcomes used to compute a cost function $C(\vec{\alpha}, \vec{\beta})$ which evaluates the effectiveness of the adopted QEC strategy in leading large values of the average input-output fidelity. The specific choice of the cost function is very important and is discussed in Section III A.
3. A classical computer decides, given the results of the measurement, how to change the value of the parameters $\vec{\alpha}$ and $\vec{\beta}$ to be used in the subsequent run in order to minimize the cost function $C(\vec{\alpha}, \vec{\beta})$. This is discussed in detail in Section III B.

A. Cost function

The natural choice for the cost function at the stage 2 of our algorithm is provided by the expectation value of the self-adjoint operator

$$\hat{H}_{QA}^{(\text{fid})} := \hat{\mathbb{1}}_{QA} - |\mathcal{O}\rangle_{QA} \langle \mathcal{O}|, \quad (6)$$

computed on the mean state of system QA which emerges at the output of the quantum circuit of Fig. 2, i.e. the quantity

$$C^{(\text{fid})}(\vec{\alpha}, \vec{\beta}) := \text{tr}\{\hat{\rho}_{QA}^{(V(\vec{\alpha}), W(\vec{\beta}))} \hat{H}_{QA}^{(\text{fid})}\}, \quad (7)$$

where $\hat{\rho}_{QA}^{(V(\vec{\alpha}), W(\vec{\beta}))}$ is the density matrix (4) evaluated for $\hat{V}_{QA} = \hat{V}_{QA}(\vec{\alpha})$ and $\hat{W}_{QAB} = \hat{W}_{QAB}(\vec{\beta})$. This choice has two main advantages. First of all, the expectation value $C^{(\text{fid})}(\vec{\alpha}, \vec{\beta})$ can be evaluated by performing (simple) local measurement on the qubits of Q and A (indeed it can be computed by simply checking whether or not each one of them is in the logical state $|0\rangle$). Most importantly, since by explicit evaluation one has that $C^{(\text{fid})}(\vec{\alpha}, \vec{\beta}) = 1 - \overline{F}(V(\vec{\alpha}), W(\vec{\beta}))$, it is clear that by using (7) the algorithm will be forced to look for values of $\vec{\alpha}, \vec{\beta}$ that yield higher average input-output fidelities. Despite all this, the use of $C^{(\text{fid})}(\vec{\alpha}, \vec{\beta})$ as a cost function, has a major drawback associated with the fact that the spectrum of the Hamiltonian $\hat{H}_{QA}^{(\text{fid})}$ exhibits maximum degeneracy with respect to space orthogonal to the target state $|\mathcal{O}\rangle_{QA}$ (see Fig. 3). Due to this fact a numerical search based on a training procedure that simply target the minimization of $C^{(\text{fid})}(\vec{\alpha}, \vec{\beta})$, has non trivial chances to get stuck somewhere in the large flat plateau associated with the eigenvalue 1 of $\hat{H}_{QA}^{(\text{fid})}$ without finding any good

direction. In the large flat plateau a possible way to avoid this problem is to introduce new cost-functions Hamiltonians which, while maintaining the target vector $|\mathcal{O}\rangle_{QA}$ as unique ground state and still being easy to compute, manage to remove the huge degeneracy of the excited part of the spectra of $\hat{H}_{QA}^{(\text{fid})}$. Our choice is based on the quantum Wasserstein distance of order 1 (W_1) introduced Ref. [63] which, even though it lacks some interesting properties that the fidelity has, is less likely to be affected by the barren plateaus phenomena [22]. A good estimation of the W_1 distance that separate $\hat{\rho}_{QA}^{(V(\vec{\alpha}), W(\vec{\beta}))}$ from the target state, is provided by the following quantity

$$C^{(\text{wass})}(\vec{\alpha}, \vec{\beta}) := \text{tr}\{\hat{\rho}_{QA}^{(V(\vec{\alpha}), W(\vec{\beta}))} \hat{H}_{QA}^{(\text{wass})}\}, \quad (8)$$

$$\hat{H}_{QA}^{(\text{wass})} := \sum_{j=1}^n j \hat{\Pi}_{QA}^{(j)}, \quad (9)$$

where $\hat{\Pi}_{QA}^{(j)}$ represents the sub-space of the register QA in which we have j qubits in $|1\rangle$ and the remaining one in $|0\rangle$. Observe that $\hat{H}_{QA}^{(\text{wass})}$ is nothing but the sum of the number operators acting on the individual qubits of the register QA , (i.e. $\hat{H}_{QA}^{(\text{wass})} = \sum_{\ell=1}^n \hat{\pi}_\ell$ with $\hat{\pi}_\ell$ the projector on the logical state $|1\rangle$ of the ℓ -th qubit): accordingly, as $C^{(\text{fid})}(\vec{\alpha}, \vec{\beta})$, $C^{(\text{wass})}(\vec{\alpha}, \vec{\beta})$ can be computed from local measurement. What $C^{(\text{wass})}(\vec{\alpha}, \vec{\beta})$ does is to count the total number of logical ones present in the system. To understand why using (8) could in principle lead to a more efficient numerical search than the one obtained by using (7), notice that Eq. (6) can be equivalently written

as $\hat{H}_{QA}^{(\text{fid})} = \sum_{j=1}^n \hat{\Pi}_{QA}^{(j)}$. A comparison with (9) reveals hence

that indeed while both $\hat{H}_{QA}^{(\text{fid})}$ and $\hat{H}_{QA}^{(\text{wass})}$ admit $|\mathcal{O}\rangle_{QA}$ as unique ground state, the Wasserstein Hamiltonian removes large part of the degeneracy of the high energy spectrum of the fidelity Hamiltonian. Accordingly it is reasonable to expect that a numerical search that uses $\hat{H}_{QA}^{(\text{wass})}$, has less chances to get trapped into regions of constant energy (barren plateau) than a search based on $\hat{H}_{QA}^{(\text{fid})}$.³

³ It goes without mentioning that alternative choices for the cost function Hamiltonians are also available. For instance one can use operators that also remove the residual degeneracies that affect $\hat{H}_{QA}^{(\text{wass})}$ – e.g. using the operator $\hat{H}_{QA}^{(\text{full})} = \sum_{\ell=1}^n w_\ell \hat{\pi}_\ell$ with w_ℓ positive weights selected so that different allocation of $|1\rangle$ states inside the eigenspaces of $\hat{H}_{QA}^{(\text{wass})}$ get an assigned ordering. Our numerical analysis however seems to indicate that these refinement do not contribute significantly in improving numerical search of the algorithm.

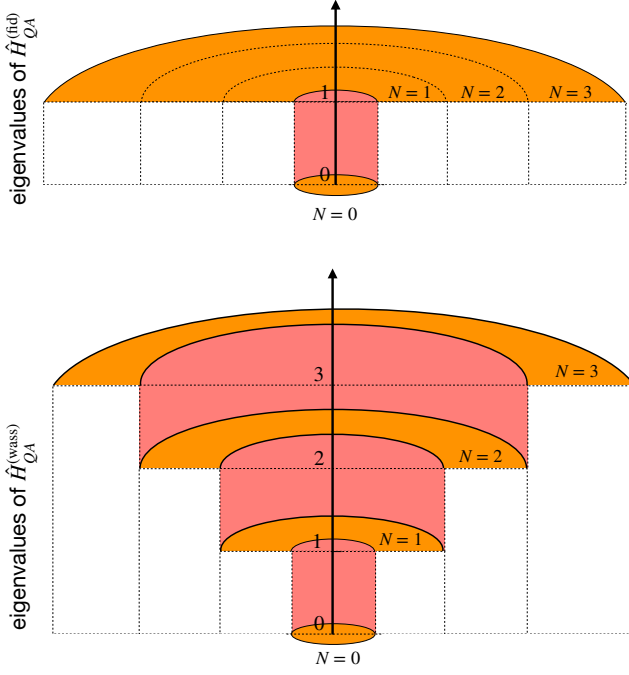


Figure 3. Pictorial rendering of the spectra of the Hamiltonians $\hat{H}_{QA}^{(fid)}$ (top panel) and $\hat{H}_{QA}^{(wass)}$ (lower panel). While $\hat{H}_{QA}^{(fid)}$ is characterized by a unique, flat plateau that includes all the excited state, $\hat{H}_{QA}^{(wass)}$ partially removes the associated degeneracy assigning higher energy to subspaces that have higher number of qubits in the logical state $|1\rangle$.

B. Descent algorithm

The algorithm that we used for this work is a gradient descent algorithm with momentum [74]. To overcome the numerical difficulties of using finite differences to estimate the gradients of the cost function $C(\vec{\alpha}, \vec{\beta})$, we exploit a variation of the parameter-shift rule introduced in [75] which reduces the problem to compute linear combinations of the function itself evaluated in different points that are not infinitesimally close. Specifically we observe that, irrespectively from the choice of the operator \hat{H}_{QA} , the functional dependence of $C(\vec{\alpha}, \vec{\beta})$ upon the j -th component of the vector $\vec{\beta}$ is of the form

$$C(\vec{\alpha}, \vec{\beta}) = f(\beta_j) := \sum_k \text{tr} \{ \hat{\Omega}_1^{(k)} e^{i\beta_j \hat{\sigma}} \hat{\Omega}_2^{(k)} e^{-i\beta_j \hat{\sigma}} \}, \quad (10)$$

with $\hat{\Omega}_{1,2}^{(k)}$ being multi-qubits operators which do not depend upon β_j , and with $e^{-i\beta_j \hat{\sigma}}$ a single qubit rotation generated by an element $\hat{\sigma}$ of the Pauli set. Therefore its gradient can be written as

$$\begin{aligned} \frac{\partial C(\vec{\alpha}, \vec{\beta})}{\partial \beta_j} &= i \sum_k \text{tr} \{ \hat{\Omega}_1^{(k)} e^{i\beta_j \hat{\sigma}} [\hat{\sigma}, \hat{\Omega}_2^{(k)}] e^{-i\beta_j \hat{\sigma}} \} \\ &= f(\beta_j + \frac{\pi}{4}) - f(\beta_j - \frac{\pi}{4}), \end{aligned} \quad (11)$$

where in the last passage we used the identity

$$i[\hat{\sigma}, \hat{\Omega}_2^{(k)}] = e^{i\frac{\pi}{4}\hat{\sigma}} \hat{\Omega}_2^{(k)} e^{-i\frac{\pi}{4}\hat{\sigma}} - e^{-i\frac{\pi}{4}\hat{\sigma}} \hat{\Omega}_2^{(k)} e^{i\frac{\pi}{4}\hat{\sigma}}. \quad (12)$$

The gradient with respect the vector $\vec{\alpha}$ can be computed similarly. In this case however we observe that, due to the fact that $\hat{\rho}_{QA}^{(V(\vec{\alpha}), W(\vec{\beta}))}(\psi)$ depends upon the parameters $\vec{\alpha}$ via $\hat{V}_{QA}(\vec{\alpha})$ and through its adjoint $\hat{V}_{QA}^\dagger(\vec{\alpha})$, the dependence of $C(\vec{\alpha}, \vec{\beta})$ upon the j -th component of $\vec{\alpha}$ is slightly more complex. Indeed in this case we have

$$C(\vec{\alpha}, \vec{\beta}) = g(\alpha_j, \alpha_j), \quad (13)$$

where $g(\alpha_j^{(1)}, \alpha_j^{(2)})$ is the function

$$\begin{aligned} g(\alpha_j^{(1)}, \alpha_j^{(2)}) &:= \sum_k \text{tr} \{ \hat{\Omega}_1^{(k)} e^{i\alpha_j^{(1)} \hat{\sigma}} \hat{\Omega}_2^{(k)} e^{-i\alpha_j^{(1)} \hat{\sigma}} \\ &\quad \times \hat{\Omega}_3^{(k)} e^{i\alpha_j^{(2)} \hat{\sigma}} \hat{\Omega}_4^{(k)} e^{-i\alpha_j^{(2)} \hat{\sigma}} \}, \end{aligned} \quad (14)$$

with $\hat{\Omega}_{1,2,3,4}^{(k)}$ representing multi-qubits operators which do not depend neither upon $\alpha_j^{(1)}$ nor $\alpha_j^{(2)}$. It is important to stress that $g(\alpha_j^{(1)}, \alpha_j^{(2)})$ can be computed using the same circuit of Fig. 2, by simply replacing the phases α_j of $\hat{V}_{QA}(\vec{\alpha})$ and $\hat{V}_{QA}^\dagger(\vec{\alpha})$ with $\alpha_j^{(1)}$ and $\alpha_j^{(2)}$ respectively. Notice finally that exploiting the identity Eq. (12) we can write

$$\begin{aligned} \frac{\partial C(\vec{\alpha}, \vec{\beta})}{\partial \alpha_j} &= \left. \frac{\partial g(\alpha_j^{(1)}, \alpha_j)}{\partial \alpha_j^{(1)}} \right|_{\alpha_j^{(1)}=\alpha_j} + \left. \frac{\partial g(\alpha_j, \alpha_j^{(2)})}{\partial \alpha_j^{(2)}} \right|_{\alpha_j^{(2)}=\alpha_j} \\ &= g(\alpha_j + \frac{\pi}{4}, \alpha_j) - g(\alpha_j - \frac{\pi}{4}, \alpha_j) \\ &\quad + g(\alpha_j, \alpha_j + \frac{\pi}{4}) - g(\alpha_j, \alpha_j - \frac{\pi}{4}), \end{aligned} \quad (15)$$

which shows that computing the gradient of $C(\vec{\alpha}, \vec{\beta})$ with respect to α_j simply accounts to evaluate the circuit that express $g(\alpha_j^{(1)}, \alpha_j^{(2)})$ for four distinct values of the parameters.

C. Noise model

The scheme presented so far can in principle be applied to arbitrary classes of noises. In our research however we focused on a specific model that has been extensively studied in the literature producing explicit examples of efficient QEC solutions which can be used as a theoretical benchmark for our variational search. Specifically we assume Q and A to be respectively a single qubit register ($k=1$) and a two qubit register ($n=3$), globally affected by a given species of single-qubit noise [76, 77]. These transformations can be represented in terms of a LCPT map of the form

$$\Phi_{QA}(\cdots) = \sum_{\ell=0}^n \hat{K}_{QA}^{(\ell)} \cdots \hat{K}_{QA}^{(\ell)\dagger}, \quad (16)$$

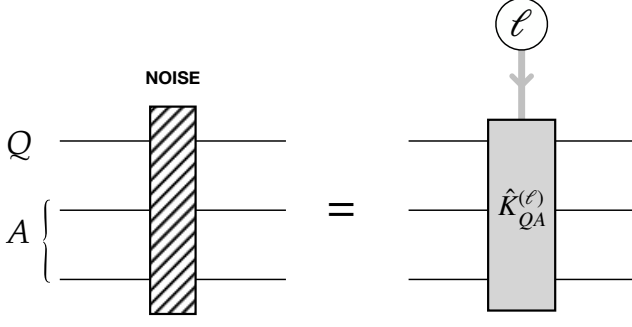


Figure 4. Circuitual implementation of the noise element of Fig. 2: here $\hat{K}_{QA}^{(\ell)}$ are weighted unitaries of Eq. (17).

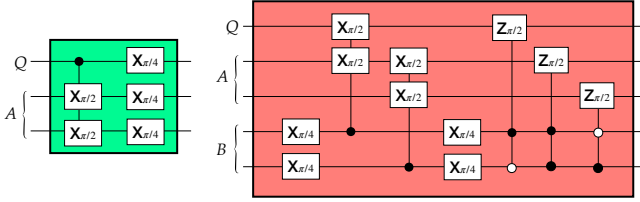


Figure 5. Circuitual implementations of the ideal transformations $\hat{V}_{QA}(\vec{\alpha})$ (left) and $\hat{W}_{QAB}(\vec{\beta})$ (right) which allow for exact noise suppression of a single-qubit bit-flip noise model [i.e. (16) with $\hat{\sigma}^{(\ell)} = \hat{\sigma}_1^{(\ell)}$] using a quantum register B with $r = 2$ qubit. Here H represent Hadamard gates, while the control-element are C-NOT gates.

with Kraus operators [71]

$$\hat{K}_{QA}^{(0)} := \sqrt{1-p} \hat{1}_{QA}, \quad \hat{K}_{QA}^{(\ell)} := \sqrt{\frac{p}{n}} \hat{\sigma}^{(\ell)}, \quad (17)$$

where for $\ell \in \{1, \dots, n\}$, $\hat{\sigma}^{(\ell)}$ is the Pauli operator acting on the ℓ -th qubit of QA which defines the noise species we have selected. For instance in the case we choose to describe phase-flip noise then $\hat{\sigma}^{(\ell)} = \hat{\sigma}_3^{(\ell)}$, while for describing bit-flip we have $\hat{\sigma}^{(\ell)} = \hat{\sigma}_1^{(\ell)}$. Explicit examples of \hat{V}_{QA} , \hat{W}_{QAB} which allow for exact suppression of the noise ($\bar{F}(V, W) = 1$) are shown in Fig. 5. Notice that by construction the circuit parametrization of $\hat{V}_{QA}(\vec{\alpha})$, $\hat{W}_{QAB}(\vec{\beta})$ given in Fig. 2 include such gates as special solution: accordingly if properly guided by an efficient cost function, our numerical VQA search has a chance to find the solution of Fig. 5.

IV. RESULTS

In this section we study the impact of the cost function on the efficiency of the optimization algorithm of Sec. III. Assuming the single-qubit noise model detailed in Sec. IIIC and taking B to be a $r = 2$ qubit register, we run two distinct numerical searches: the first obtained

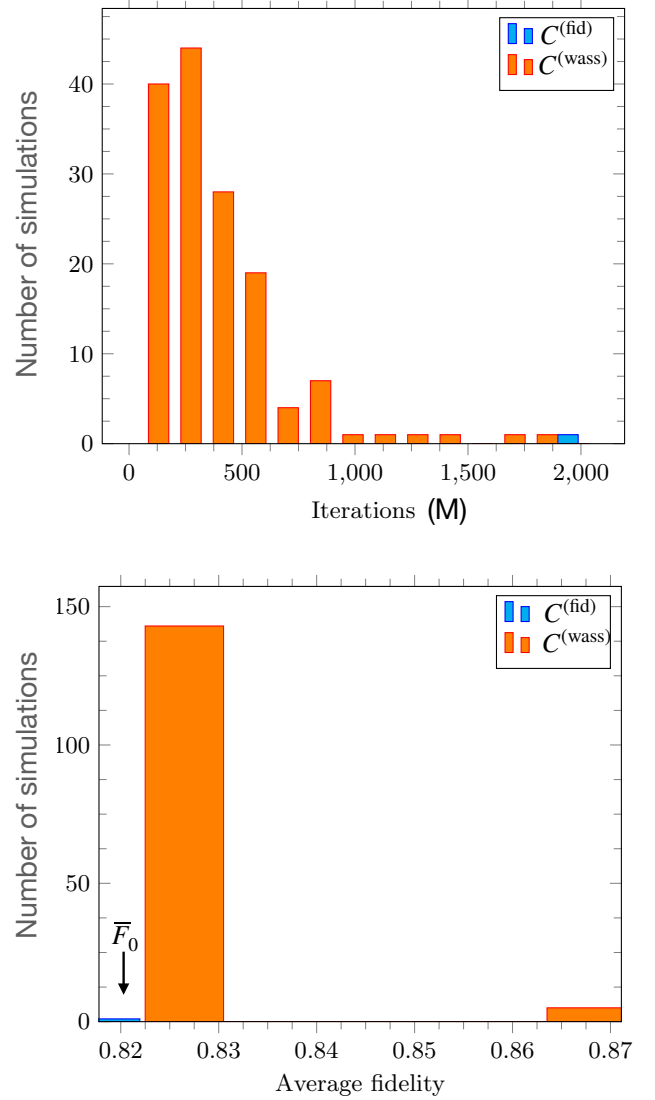


Figure 6. Comparison of the the input-output average fidelity (3) attainable by running our optimization algorithm using the cost function $C^{(\text{fid})}(\vec{\alpha}, \vec{\beta})$ (blue data) and $C^{(\text{wass})}(\vec{\alpha}, \vec{\beta})$ (orange data). Here the error model is a single-qubit bit-flip noise ($\hat{\sigma} = \hat{\sigma}_1$ in (16)) with $p = 0.8$. The no error correction threshold (5) of this scheme is $\bar{F}_0 \approx 0.822$ – orange peak in the fidelity plot, up to numerical precision. Only the runs that produced a fidelity of at least \bar{F}_0 have been included. For the $C^{(\text{fid})}(\vec{\alpha}, \vec{\beta})$ this is 0.2%, while for $C^{(\text{wass})}(\vec{\alpha}, \vec{\beta})$ this corresponds to 29.6%.

by identifying $C(\vec{\alpha}, \vec{\beta})$ with $C^{(\text{fid})}(\vec{\alpha}, \vec{\beta})$ and the second choosing instead $C^{(\text{wass})}(\vec{\alpha}, \vec{\beta})$. Results are reported in Figs. 6 and 7 for two different choices of the noise models (16), i.e. phase-flip and bit-flip. For both we compare the input-output average fidelity (3) at the end of the procedure obtained with the two different cost functions, and the number of iterations M needed for convergence. Regarding this last quantity we set a maximum value M_{max} equal to 2000 before convergence and we chose this

limit mainly with practical choices like the maximum time for the simulation, enforcing that a single run does not require more than a few hours of computational time: in case the algorithm fails to reach the convergency we simply stop the numerical search (this is the reason for the peak at the end of the upper orange plot in Fig. 7). The plots report only the simulations that manage to achieve an average fidelity that is greater or equal than no-correction threshold bound \bar{F}_0 .

The first thing to observe is that for both noise models, $C^{(\text{fid})}(\vec{\alpha}, \vec{\beta})$ has problem in reaching the do-nothing threshold \bar{F}_0 : the probability of success being 2.6% for the phase-flip case of Fig. 7 and only 0.2% for the bit-flip case of Fig. 6 (for both noise models the total number of simulations analyzed was 500). Observe also that in this last case the algorithm never yields average input-output fidelity values strictly larger than \bar{F}_0 and that, even in those cases, it requires a number M of iterations which saturate the maximum allow value M_{max} (blue peak in the upper plot of Fig. 7). $C^{(\text{wass})}(\vec{\alpha}, \vec{\beta})$ performs definitely better: to begin with it succeeds in overcoming the threshold \bar{F}_0 in one third of the simulations (specifically 40.6% for the phase-flip noise model and 29.6% for the bit-flip noise model). Furthermore the algorithm reach convergency with a number of iterations which are typically smaller than those required by $C^{(\text{fid})}(\vec{\alpha}, \vec{\beta})$.

To better enlighten the differences between the two cost functions, we proceeded with further simulations, whose results are summarized in Fig. 8. The idea here is to run a two-step optimization process composed by two sequences of runs: in the first run we start the optimization procedure from a random point in the parameter space $(\vec{\alpha}, \vec{\beta})$ with one of the two cost functions (say $C^{(\text{fid})}(\vec{\alpha}, \vec{\beta})$), up to convergence; after that we start a second optimization run using the other cost function (say $C^{(\text{wass})}(\vec{\alpha}, \vec{\beta})$) but assuming as initial condition for the parameters the final point reached by the first run. The plots report the difference in fidelity between the second and the first run: when we start using the $C^{(\text{wass})}(\vec{\alpha}, \vec{\beta})$ in the first run, the fidelity cannot further improve the result that is already found, and this is represented by the fact that the best improvement is of the order of 10^{-5} ; on the contrary if we started employing $C^{(\text{fid})}(\vec{\alpha}, \vec{\beta})$ in the first run, the use of $C^{(\text{wass})}(\vec{\alpha}, \vec{\beta})$ in the second run typically yields substantial improvements of the performance⁴. Moreover, we sampled some single descent processes and plotted the cost in function of the iteration. When we move from

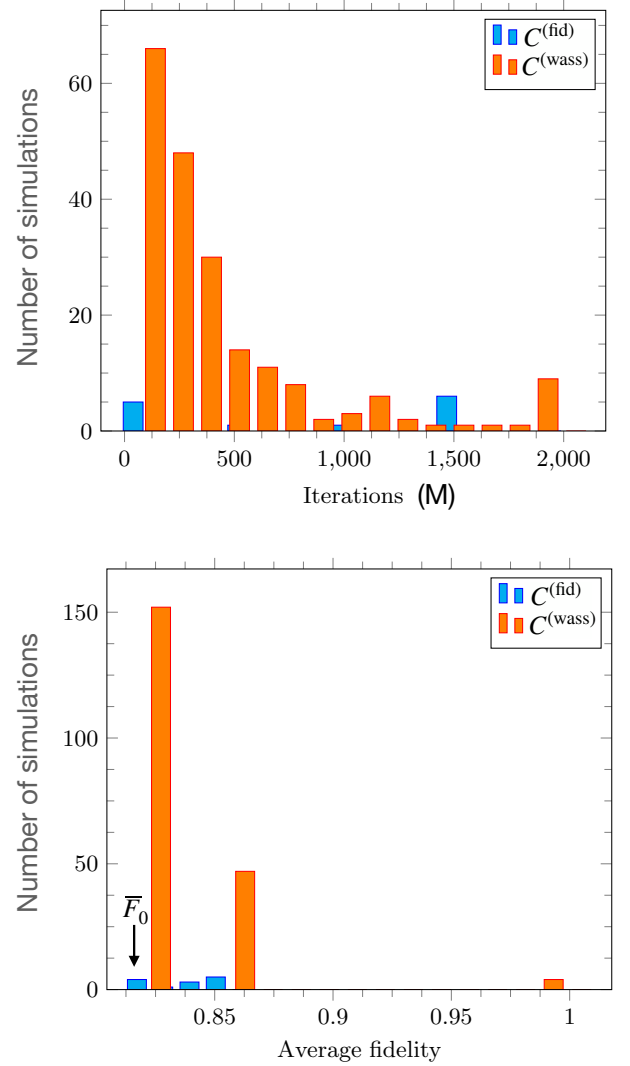


Figure 7. Comparison of the the input-output average fidelity (3) attainable by running our optimization algorithm using the cost function $C^{(\text{fid})}(\vec{\alpha}, \vec{\beta})$ (blue data) and $C^{(\text{wass})}(\vec{\alpha}, \vec{\beta})$ (orange data). Here the error model is a single-qubit phase-flip noise ($\hat{\sigma} = \hat{\sigma}_3$ in (16) with $p = 0.8$). The no error correction threshold (5) of this scheme is $\bar{F}_0 \approx 0.822$ – orange peak in the fidelity plot, up to numerical precision. Only the runs that produced a fidelity of at least \bar{F}_0 have been included. For the $C^{(\text{fid})}(\vec{\alpha}, \vec{\beta})$ this is 2.6%, while for $C^{(\text{wass})}(\vec{\alpha}, \vec{\beta})$ this corresponds to 40.6%.

fidelity to W_1 , the descent part after the change of cost function is qualitatively indistinguishable from starting from a random point.

⁴ It has to be said that in few cases the figure of merit is worse after the second optimization – see the negative bar in right panel of Fig. 8. This is due to the fact that when using $C^{(\text{wass})}(\vec{\alpha}, \vec{\beta})$ we are not maximizing the fidelity but minimizing a function whose stationary point corresponds to the maximum of the latter: accordingly the final point of convergence for $C^{(\text{wass})}(\vec{\alpha}, \vec{\beta})$ can

be slightly off mark in terms of fidelity. This is not a problem because these two functions do not have a constant ratio, and we checked that the inequalities between them are still satisfied.

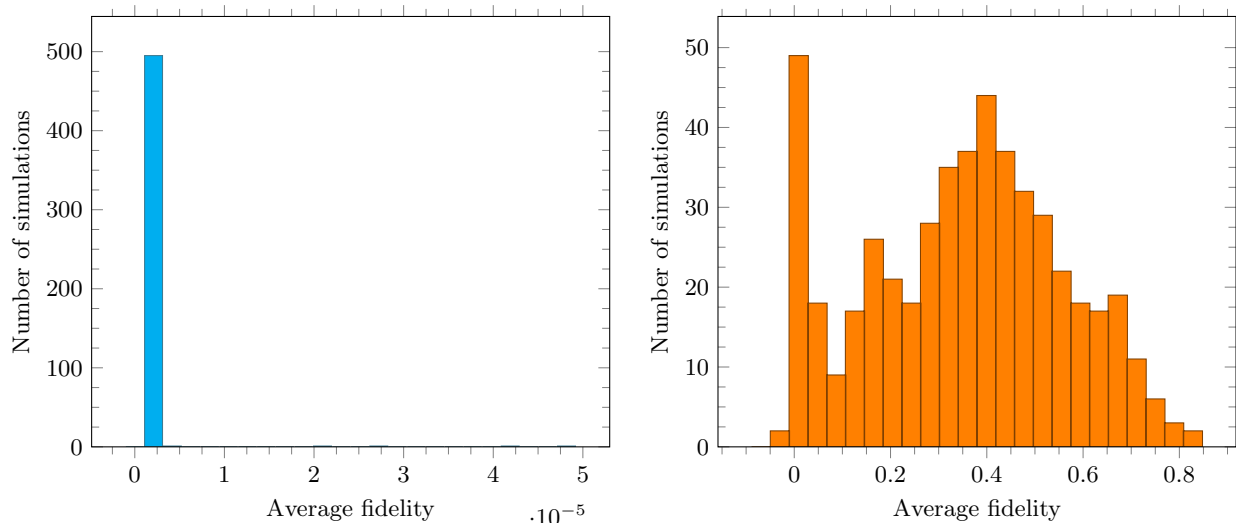


Figure 8. Improvement of simulations when changing the cost function in a two run optimization process that uses different cost functions to drive the descent algorithm. In the left plot, we started the descent on a random initial point, ran the optimization using $C^{(\text{wass})}(\vec{\alpha}, \vec{\beta})$ as cost function until convergence and then we started the descent algorithm again but using $C^{(\text{fid})}(\vec{\alpha}, \vec{\beta})$ as cost function, starting from the final point of the previous descent. In the right part, the roles of the two cost functions are inverted (we start using $C^{(\text{fid})}(\vec{\alpha}, \vec{\beta})$ and then we use $C^{(\text{wass})}(\vec{\alpha}, \vec{\beta})$). The histograms represent the difference in average input-output fidelity (2) after the change of cost function, namely the difference between the fidelity achieved after the second descent and the fidelity after the first descent (positive values correspond to improved performances). Please notice the scale difference on the x -axis between the left and right plot.

V. CONCLUSIONS

To summarize, we have shown a variational quantum algorithm that allows finding the most suitable error correction procedure for a specific noise on quantum hardware. We compared the performance of two different versions of this algorithm using two different cost functions, the fidelity and an approximation of the quantum Wasserstein distance of order one. We compared the difference in speed and the ability to obtain a useful solution between the two algorithms, finding really different trends between the two optimization procedures. The optimization process based on the fidelity suffers greatly from the phenomenon of the barren plateaus, leading to very slow convergence or no convergence at all, while the algorithm based on the quantum W_1 distance allows us to find the configurations that correct the errors in the examples that we explored. The obtained results show a clear improvement and allow us to explore further improvements of these methods, as using different algorithms for the minimization process, e.g. stochastic gradient descent or higher-order algorithms like Newton or pseudo-Newton algorithms.

Given that the gradient can be expressed only with the cost function evaluated in a small number of circuits that differ only in the parameter choice, the gradient of the cost function can be computed on the same hardware that will be used for the correction procedure. Moreover, simulating this circuit may be difficult because of the exponential scaling of the dimension of the Hilbert space

of a set of qubits, but this problem does not apply when all the circuit is built on hardware, gaining a quantum advantage. For the same reason, the same procedure can be iterated to compute the exact Hessian of the cost function and then apply a second-order method like the Newton method as a descent algorithm. However, this has not been done because the circuits that we marked as useful have a relatively big number of parameters, and computing the hessian scales quadratically with this number, leading to intractable computations.

Acknowledgments

FZ and VG acknowledge financial support by MIUR (Ministero dell' Istruzione, dell' Università della Ricerca) by PRIN 2017 Taming complexity via Quantum Strategies: a Hybrid Integrated Photonic approach (QUSHIP) Id. 2017SRN-BRK, and via project PRO3 Quantum Pathfinder. GDP is a member of the “Gruppo Nazionale per la Fisica Matematica (GNFM)” of the “Istituto Nazionale di Alta Matematica “Francesco Severi” (INdAM)”.

VI. BIBLIOGRAPHY

- [1] J. W. Z. Lau, K. H. Lim, H. Shrotriya, and L. C. Kwek, Nisq computing: where are we and where do we go?, *AAPPS Bulletin* **32**, 27 (2022).

- [2] J. Preskill, [Quantum computing and the entanglement frontier](#) (2012).
- [3] J. Preskill, Quantum computing in the NISQ era and beyond, [Quantum](#) **2**, 79 (2018).
- [4] N. Gisin, G. Ribordy, W. Tittel, and H. Zbinden, Quantum cryptography, [Reviews of Modern Physics](#) **74**, 145 (2002).
- [5] H.-K. Lo, M. Curty, and K. Tamaki, Secure quantum key distribution, [Nature Photonics](#) **8**, 595 (2014).
- [6] K. Banaszek, Optimal receiver for quantum cryptography with two coherent states, [Physics Letters A](#) **253**, 12 (1999).
- [7] S. Pirandola, U. L. Andersen, L. Banchi, M. Berta, D. Bunandar, R. Colbeck, D. Englund, T. Gehring, C. Lupo, C. Ottaviani, J. L. Pereira, M. Razavi, J. S. Shaari, M. Tomamichel, V. C. Usenko, G. Vallone, P. Villoresi, and P. Wallden, Advances in quantum cryptography, [Adv. Opt. Photon.](#) **12**, 1012 (2020).
- [8] F. Cavaliere, E. Prati, L. Poti, I. Muhammad, and T. Catuogno, Secure quantum communication technologies and systems: From labs to markets, [Quantum Reports](#) **2**, 80 (2020).
- [9] E. Knill, R. Laflamme, R. Martinez, and C. Negrevergne, Implementation of the five qubit error correction benchmark, arXiv preprint quant-ph/0101034 (2001).
- [10] A. S. Fletcher, P. W. Shor, and M. Z. Win, Channel-adapted quantum error correction for the amplitude damping channel, [IEEE Transactions on Information Theory](#) **54**, 5705 (2008).
- [11] R. L. Kosut, A. Shabani, and D. A. Lidar, Robust quantum error correction via convex optimization, [Phys. Rev. Lett.](#) **100**, 020502 (2008).
- [12] S. Taghavi, R. L. Kosut, and D. A. Lidar, Channel-optimized quantum error correction, [IEEE Transactions on Information Theory](#) **56**, 1461 (2010).
- [13] M. Chiani and L. Valentini, Short Codes for Quantum Channels With One Prevalent Pauli Error Type, [IEEE Journal on Selected Areas in Information Theory](#) **1**, 480 (2020).
- [14] J. Koch, T. M. Yu, J. Gambetta, A. A. Houck, D. I. Schuster, J. Majer, A. Blais, M. H. Devoret, S. M. Girvin, and R. J. Schoelkopf, Charge-insensitive qubit design derived from the cooper pair box, [Physical Review A](#) **76**, 042319 (2007).
- [15] M. J. Peterer, S. J. Bader, X. Jin, F. Yan, A. Kamal, T. J. Gudmundsen, P. J. Leek, T. P. Orlando, W. D. Oliver, and S. Gustavsson, Coherence and decay of higher energy levels of a superconducting transmon qubit, [Phys. Rev. Lett.](#) **114**, 010501 (2015).
- [16] S. Boixo, S. V. Isakov, V. N. Smelyanskiy, R. Babbush, N. Ding, Z. Jiang, M. J. Bremner, J. M. Martinis, and H. Neven, Characterizing quantum supremacy in near-term devices, [Nature Physics](#) **10.1038/s41567-018-0124-x** (2018).
- [17] M. Cerezo, A. Arrasmith, R. Babbush, S. C. Benjamin, S. Endo, K. Fujii, J. R. McClean, K. Mitarai, X. Yuan, L. Cincio, and et al., Variational quantum algorithms, [Nature Reviews Physics](#) **3**, 625–644 (2021).
- [18] J. Tilly, H. Chen, S. Cao, D. Picozzi, K. Setia, Y. Li, E. Grant, L. Wossnig, I. Rungger, G. H. Booth, and J. Tennyson, [The variational quantum eigensolver: a review of methods and best practices](#) (2021).
- [19] S. Hadfield, Z. Wang, B. O’Gorman, E. Rieffel, D. Venturelli, and R. Biswas, From the quantum approximate optimization algorithm to a quantum alternating operator ansatz, [Algorithms](#) **12**, 34 (2019).
- [20] P. D. Johnson, J. Romero, J. Olson, Y. Cao, and A. Aspuru-Guzik, Qvector: an algorithm for device-tailored quantum error correction (2017), [arXiv:1711.02249 \[quant-ph\]](#).
- [21] J. R. McClean, S. Boixo, V. N. Smelyanskiy, R. Babbush, and H. Neven, Barren plateaus in quantum neural network training landscapes, [Nature Communications](#) **10.1038/s41467-018-07090-4** (2018).
- [22] M. Cerezo, A. Sone, T. Volkoff, L. Cincio, and P. J. Coles, Cost function dependent barren plateaus in shallow parametrized quantum circuits, [Nature Communications](#) **10.1038/s41467-021-21728-w** (2021).
- [23] G. Monge, *Mémoire sur la théorie des déblais et des remblais* (Mémoires de l’Académie royale des sciences de Paris vol 1781, 1781) p. 625–704.
- [24] L. V. Kantorovich, On the translocation of masses, [Journal of Mathematical Sciences](#) **133**, 1381 (2006).
- [25] L. Ambrosio, Gradient flows in metric spaces and in the spaces of probability measures, and applications to fokker-planck equations with respect to log-concave measures, [Bollettino dell’Unione Matematica Italiana](#) **1**, 223 (2008).
- [26] G. Peyré and M. Cuturi, Computational optimal transport: With applications to data science, [Foundations and Trends® in Machine Learning](#) **11**, 355 (2019).
- [27] A. M. Vershik, Long history of the monge-kantorovich transportation problem, [The Mathematical Intelligencer](#) **35**, 1 (2013).
- [28] E. A. Carlen and J. Maas, An analog of the 2-Wasserstein metric in non-commutative probability under which the Fermionic Fokker–Planck equation is gradient flow for the entropy, [Communications in Mathematical Physics](#) **331**, 887 (2014).
- [29] E. A. Carlen and J. Maas, Gradient flow and entropy inequalities for quantum Markov semigroups with detailed balance, [Journal of Functional Analysis](#) **273**, 1810 (2017).
- [30] E. A. Carlen and J. Maas, Non-commutative calculus, optimal transport and functional inequalities in dissipative quantum systems, [Journal of Statistical Physics](#) **178**, 319 (2020).
- [31] C. Rouzé and N. Datta, Concentration of quantum states from quantum functional and transportation cost inequalities, [Journal of Mathematical Physics](#) **60**, 012202 (2019).
- [32] N. Datta and C. Rouzé, Relating relative entropy, optimal transport and Fisher information: A quantum HWI inequality, [Annales Henri Poincaré](#) **21**, 2115 (2020).
- [33] T. Van Vu and Y. Hasegawa, Geometrical Bounds of the Irreversibility in Markovian Systems, [Phys. Rev. Lett.](#) **126**, 010601 (2021).
- [34] M. Wirth, A dual formula for the noncommutative transport distance, [Journal of Statistical Physics](#) **187**, 1 (2022).
- [35] L. Gao, M. Junge, and N. LaRacuente, Fisher information and logarithmic sobolev inequality for matrix-valued functions, [Annales Henri Poincaré](#) **21**, 3409 (2020).
- [36] Y. Chen, T. T. Georgiou, L. Ning, and A. Tannenbaum, Matricial Wasserstein-1 distance, [IEEE control systems letters](#) **1**, 14 (2017).
- [37] E. K. Ryu, Y. Chen, W. Li, and S. Osher, Vector and matrix optimal mass transport: theory, algorithm, and applications, [SIAM Journal on Scientific Computing](#) **40**, A3675 (2018).
- [38] Y. Chen, T. T. Georgiou, and A. Tannenbaum, Matrix optimal mass transport: a quantum mechanical approach,

- IEEE Transactions on Automatic Control **63**, 2612 (2018).
- [39] Y. Chen, T. T. Georgiou, and A. Tannenbaum, Wasserstein geometry of quantum states and optimal transport of matrix-valued measures, in *Emerging Applications of Control and Systems Theory* (Springer, 2018) pp. 139–150.
- [40] J. Agredo, A Wasserstein-type distance to measure deviation from equilibrium of quantum Markov semigroups, *Open Systems & Information Dynamics* **20**, 1350009 (2013).
- [41] J. Agredo, On exponential convergence of generic quantum Markov semigroups in a Wasserstein-type distance, *International Journal of Pure and Applied Mathematics* **107**, 909 (2016).
- [42] K. Ikeda, Foundation of quantum optimal transport and applications, *Quantum Information Processing* **19**, 25 (2020).
- [43] F. Golse, C. Mouhot, and T. Paul, On the mean field and classical limits of quantum mechanics, *Communications in Mathematical Physics* **343**, 165 (2016).
- [44] E. Caglioti, F. Golse, and T. Paul, Towards Optimal Transport for Quantum Densities, arXiv:2101.03256 [10.48550/ARXIV.2101.03256](https://arxiv.org/abs/2101.03256) (2021).
- [45] F. Golse, The quantum N-body problem in the mean-field and semiclassical regime, *Philosophical Transactions of the Royal Society A: Mathematical, Physical and Engineering Sciences* **376**, 20170229 (2018).
- [46] F. Golse and T. Paul, The Schrödinger equation in the mean-field and semiclassical regime, *Archive for Rational Mechanics and Analysis* **223**, 57 (2017).
- [47] F. Golse and T. Paul, Wave packets and the quadratic Monge–Kantorovich distance in quantum mechanics, *Comptes Rendus Mathématique* **356**, 177 (2018).
- [48] E. Caglioti, F. Golse, and T. Paul, Quantum optimal transport is cheaper, *Journal of Statistical Physics* **181**, 149 (2020).
- [49] S. Friedland, M. Eckstein, S. Cole, and K. Życzkowski, Quantum Monge–Kantorovich Problem and Transport Distance between Density Matrices, *Phys. Rev. Lett.* **129**, 110402 (2022).
- [50] S. Cole, M. Eckstein, S. Friedland, and K. Życzkowski, Quantum Optimal Transport, arXiv:2105.06922 [10.48550/ARXIV.2105.06922](https://arxiv.org/abs/2105.06922) (2021).
- [51] R. Duvenhage, Optimal quantum channels, *Phys. Rev. A* **104**, 032604 (2021).
- [52] R. Bistron, M. Eckstein, and K. Życzkowski, Monotonicity of the quantum 2-Wasserstein distance, arXiv:2204.07405 [10.48550/ARXIV.2204.07405](https://arxiv.org/abs/2204.07405) (2022).
- [53] T. Van Vu and K. Saito, Thermodynamic Unification of Optimal Transport: Thermodynamic Uncertainty Relation, Minimum Dissipation, and Thermodynamic Speed Limits, arXiv preprint arXiv:2206.02684 (2022).
- [54] R. Duvenhage, Quadratic Wasserstein metrics for von Neumann algebras via transport plans, arXiv:2012.03564 [10.48550/ARXIV.2012.03564](https://arxiv.org/abs/2012.03564) (2020).
- [55] R. Duvenhage, Wasserstein distance between non-commutative dynamical systems, arXiv:2112.12532 [10.48550/ARXIV.2112.12532](https://arxiv.org/abs/2112.12532) (2021).
- [56] R. Duvenhage, S. Skosana, and M. Snyman, Extending quantum detailed balance through optimal transport, arXiv preprint arXiv:2206.15287 (2022).
- [57] G. De Palma and D. Trevisan, Quantum optimal transport with quantum channels, *Annales Henri Poincaré* **22**, 3199 (2021).
- [58] R. Duvenhage and M. Snyman, Balance between quantum Markov semigroups, *Annales Henri Poincaré* **19**, 1747 (2018).
- [59] J. Agredo and F. Fagnola, On quantum versions of the classical Wasserstein distance, *Stochastics* **89**, 910 (2017).
- [60] K. Życzkowski and W. Słomczynski, The Monge distance between quantum states, *Journal of Physics A: Mathematical and General* **31**, 9095 (1998).
- [61] K. Życzkowski and W. Słomczynski, The Monge metric on the sphere and geometry of quantum states, *Journal of Physics A: Mathematical and General* **34**, 6689 (2001).
- [62] I. Bengtsson and K. Życzkowski, *Geometry of Quantum States: An Introduction to Quantum Entanglement* (Cambridge University Press, 2017).
- [63] G. De Palma, M. Marvian, D. Trevisan, and S. Lloyd, The quantum wasserstein distance of order 1, *IEEE Transactions on Information Theory* **67**, 6627 (2021).
- [64] B. T. Kiani, G. D. Palma, M. Marvian, Z.-W. Liu, and S. Lloyd, Learning quantum data with the quantum earth mover’s distance, *Quantum Science and Technology* **7**, 045002 (2022).
- [65] R. W. Hamming, Error detecting and error correcting codes, *The Bell System Technical Journal* **29**, 147 (1950).
- [66] L. Kim, S. Lloyd, and M. Marvian, Hamiltonian Quantum Generative Adversarial Networks [10.48550/ARXIV.2211.02584](https://arxiv.org/abs/2211.02584) (2022).
- [67] D. Herr, B. Obert, and M. Rosenkranz, Anomaly detection with variational quantum generative adversarial networks, *Quantum Science and Technology* **6**, 045004 (2021).
- [68] E. R. Anschuetz and B. T. Kiani, Beyond Barren Plateaus: Quantum Variational Algorithms Are Swamped With Traps, arXiv:2205.05786 [10.48550/ARXIV.2205.05786](https://arxiv.org/abs/2205.05786) (2022).
- [69] B. Coyle, *Machine learning applications for noisy intermediate-scale quantum computers*, Ph.D. thesis, University of Edinburgh (2022).
- [70] S. Chakrabarti, H. Yiming, T. Li, S. Feizi, and X. Wu, Quantum wasserstein generative adversarial networks, in *Advances in Neural Information Processing Systems* (2019) pp. 6781–6792.
- [71] M. A. Nielsen and I. L. Chuang, *Quantum Computation and Quantum Information* (Cambridge University Press, 2000).
- [72] E. B. Vinberg, *Linear representations of groups* (Boston: Birkhauser Verlag, 1989).
- [73] C. Dankert, R. Cleve, J. Emerson, and E. Livine, Exact and approximate unitary 2-designs and their application to fidelity estimation, *Physical Review A* **80**, 012304 (2009).
- [74] J. Nocedal and S. J. Wright, *Numerical Optimization*, 2nd ed. (Springer, New York, NY, USA, 2006).
- [75] M. Schuld, V. Bergholm, C. Gogolin, J. Izaac, and N. Killoran, Evaluating analytic gradients on quantum hardware, *Physical Review A* **99**, 032331 (2019).
- [76] D. Gottesman, *An introduction to quantum error correction and fault-tolerant quantum computation* (2009).
- [77] E. Knill, R. Laflamme, R. Martinez, and C. Negrevergne, Benchmarking quantum computers: The five-qubit error correcting code, *Physical Review Letters* **86**, 5811 (2001).